IEEE Access
Multidisciplinary | Rapid Review | Open Access Journal

Received 11 March 2024, accepted 3 May 2024, date of publication 9 May 2024, date of current version 10 June 2024.

Digital Object Identifier 10.1109/ACCESS.2024.3399483

RESEARCH ARTICLE

Lifetime Optimization of Optical Sensing System With Highly Reliable a-Si:H TFT-Based Optical Sensor and Driver Circuit in Large AMLCDs

CHIH-LUNG LIN[1], (Senior Member, IEEE), CHIA-LUN LEE[1], CHENG-HAN KE[1], PO-CHENG LAI[2], CHUNG-TIEN CHIU[1], YU-CHANG CHIU[1], AND CHIA-WEI KUO[2]

[1]Department of Electrical Engineering, National Cheng Kung University, Tainan 70101, Taiwan
[2]AUO Corporation, Hsinchu 30078, Taiwan

Corresponding author: Chih-Lung Lin (cllin@ee.ncku.edu.tw)

This work was supported in part by the National Science and Technology Council under Project NSTC 112-2218-E-006-010-MBK, and in part by AUO Corporation.

ABSTRACT This paper presents a lifetime optimization of optical sensing system that integrates highly reliable optical sensors and driver circuits that use hydrogenated amorphous silicon thin-film transistors (a-Si:H TFTs) to realize binary detection of optical signal with a multi-position sensing function for use in large active-matrix liquid crystal display (AMLCD). The optical sensor suppresses the effect of variations in ambient white light using a white-light photocurrent gating (WPCG) structure and increases the reliability of two photo TFTs by halving the drain-to-source voltage (V_{DS}) stress. The driver circuit switches two driving TFTs between their two modes to recover the threshold voltage (V_{TH}) shifts during a long sensing period or generate an output waveform with a large pulse width for driving the optical sensor. Experimental results indicate that the degradation of the photocurrent of the photo TFT is suppressed from 3.71 nA to 1.03 nA, representing an improvement of 72.2% relative to the original WPCG structure. The minimum difference between the output voltages of the optical sensing systems with and without an optical signal under illumination by ambient white light from 500 to 10000 lux is 18.58 V. According to an accelerated lifetime test, the feasibility of using the optical sensing system in large AMLCDs is verified.

INDEX TERMS Driver circuit, hydrogenated amorphous silicon thin-film transistors (a-Si:H TFTs), optical sensor.

I. INTRODUCTION

Hydrogenated amorphous silicon thin-film transistor (a-Si:H TFT) backplane is mainstream technology for use in large active-matrix liquid crystal displays (AMLCD), being simple to implement at low-cost and highly uniform [1], [2], [3], [4], [5], [6]. Furthermore, high sensitivity to visible light of a-Si:H TFT is also widely applied in LCD applications to support backlighting, fingerprint sensing, X-ray image generation, and optical input functions for providing several value-added functions [7], [8], [9], [10], [11]. Thus, the in-cell touch panel using optical sensors that are based on a-Si:H TFTs can perform multi-position sensing functions without any additional photolithographic mask or processing step in the fabrication and increasing the complexity of the position sensing algorithms [12], [13]. Unlike the mainstream capacitive touch panel, users can use the optical signal from a long distance to achieve contactless detection and innovate interactive applications. Abileah et al. proposed a conventional optical sensor, shown in Fig. 1(a), that consists of one a-Si:H photo TFT, one storage capacitor, and one a-Si:H switching TFT [14]. The photo TFT generates a photocurrent that depends on the intensity of the optical signal, and the voltage stored in the storage capacitor of the optical sensor is discharged to a low voltage with the optical signal or maintains the original voltage without the optical signal. The differences between the voltages represent the number of the stored charges that are further transferred to an external

The associate editor coordinating the review of this manuscript and approving it for publication was Md. Selim Habib.

charge amplifier by the switching TFT to realize binary detection of the optical signal. However, since ambient white light is an optical signal that causes the photo TFT to generate the photocurrent, affecting the sensing result, a conventional sensor under intense ambient white light cannot detect the optical signal. Therefore, our previous work [12] integrated conventional a-Si:H photo TFTs and color filter technologies to realize the white-light photocurrent gating (WPCG) structures that can reduce the effect of ambient white light and increase the number of types of optical signal from one to three. The original WPCG structure consists of three photo TFTs that are covered with red, green, and blue filters, allowing the photo TFT to generate only the photocurrent that is associated with the light of the corresponding color. One photo TFT generates the sensing photocurrent to enable the detection of the optical signal, while the two other photo TFTs generate the compensating photocurrent that suppresses the effect of the ambient light on the detection result of the optical sensor. Although the original WPCG structure in Fig. 1(b) prevents false detection, the sensing photo TFT suffers from severe stress from the high drain-to-source voltage (V_{DS}) under illumination by ambient white light during the sensing period [15], [16]. The reduced photocurrent of the degraded sensing photo TFT cannot charge the storage capacitor to a high voltage to generate a sufficient voltage difference for determining whether an optical signal is being input. Thus, a more robust optical sensing function in large AMLCD is required for design. Figs. 1 (c) and 1 (d) presented two methods for improving the reliability of an optical sensor by halving the stress time or using negative gate-to-source voltage (V_{GS}) stress in the sensing photo TFT. However, the methods that require two sets of Sn driver circuits are more costly owing to the use of additional external driver integrated circuits (ICs) and increased power consumption. Furthermore, to improve the lifetime of the optical sensing system, the reliability of the driver circuit must be considered. Although several driver circuits that are based on a-Si:H TFTs have been proposed to provide reliable output waveforms [5], [17], [18], [19], [20], these are unsuitable for generating output waveforms with a large pulse width for integration with our proposed optical sensors. These driver circuits only consider the stability of the pull-down TFT. In generating the output waveforms with a large pulse width, the driving TFT of the driver circuit suffers from more severe stress during the long sensing period. Consequently, for a lifetime optimization of optical sensing system, the designs require both a new optical sensor that suppresses the degradation of the photo TFT and a new a-Si:H driver circuit that generates stable output waveforms with a large pulse width.

This work proposes new optical sensors and driver circuits for an optical sensing system in large AMLCDs. The proposed optical sensor with a series-connected structure of sensing photo TFTs halves the V_{DS} stress, thereby reducing the degradation of the photocurrent and increasing the lifetime of the sensing photo TFTs. The optical sensor needs to be driven by only one Sn driver circuit, reducing the number of

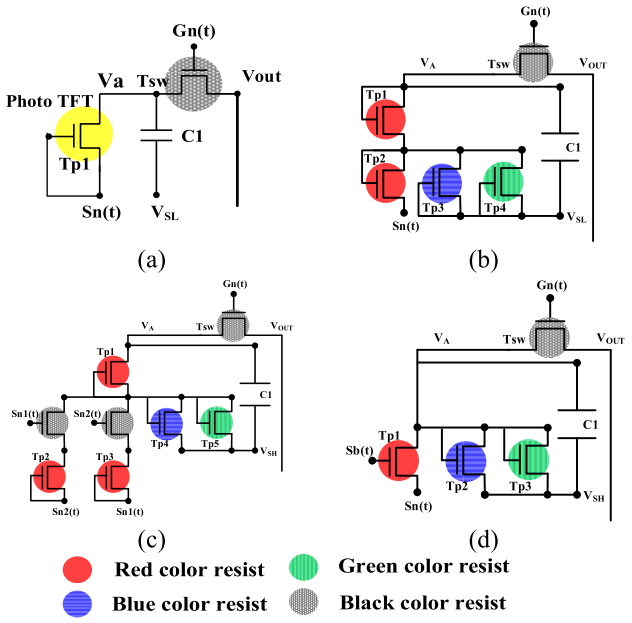

FIGURE 1. Conventional optical sensor (a) [14] and previously developed WPCG structure proposed in (b) [12]. (c) [15]. (d) [16].

ICs. Moreover, the developed Sn driver circuit uses a leakage current prevention structure to maintain the driving capability of the driving TFT and generates the required output waveforms of the optical sensor with a large pulse width. The driver circuit can switch two driving TFTs between their two modes to produce the output waveforms to drive the optical sensor or recover the threshold voltage (V_{TH}) shift that was caused by the negative bias stress, increasing the reliability of the driving TFTs and the generated output waveforms. The experimental results demonstrate that the minimum difference in the output voltage of the optical sensor is 16.06 V as the measured temperatures increase from 30 °C to 70 °C. Furthermore, the voltage drops of the output waveforms of the driver circuit are less than 1.87 % between two consecutive frames after long-term operation for 576 h. The minimum difference between the output voltages of the optical sensor with and without the optical signal is 18.58 V under illumination by the ambient white light following an accelerated lifetime test, which suffices to realize binary detection of the optical signal. The proposed optical sensor and driver circuit can be successfully integrated into a large AMLCD, as shown in Fig. 2.

II. PROPOSED OPTICAL SENSING SYSTEM

A. PROPOSED OPTICAL SENSOR AND ITS OPERATION

Fig. 3 presents a cross-sectional view of the standard a-Si:H TFT with a conventional bottom gate structure and color filters. The thickness of color resists is about 1.2 μm. The air gap of the photo TFT is about 4 μm, and the thickness of the a-Si:H film in the sensors is around 180 nm. Figs. 4(a), 4(b), and 4(c) show three proposed optical sensors with the new WPCG structure consisting of four photo TFTs. Fig. 4(d)

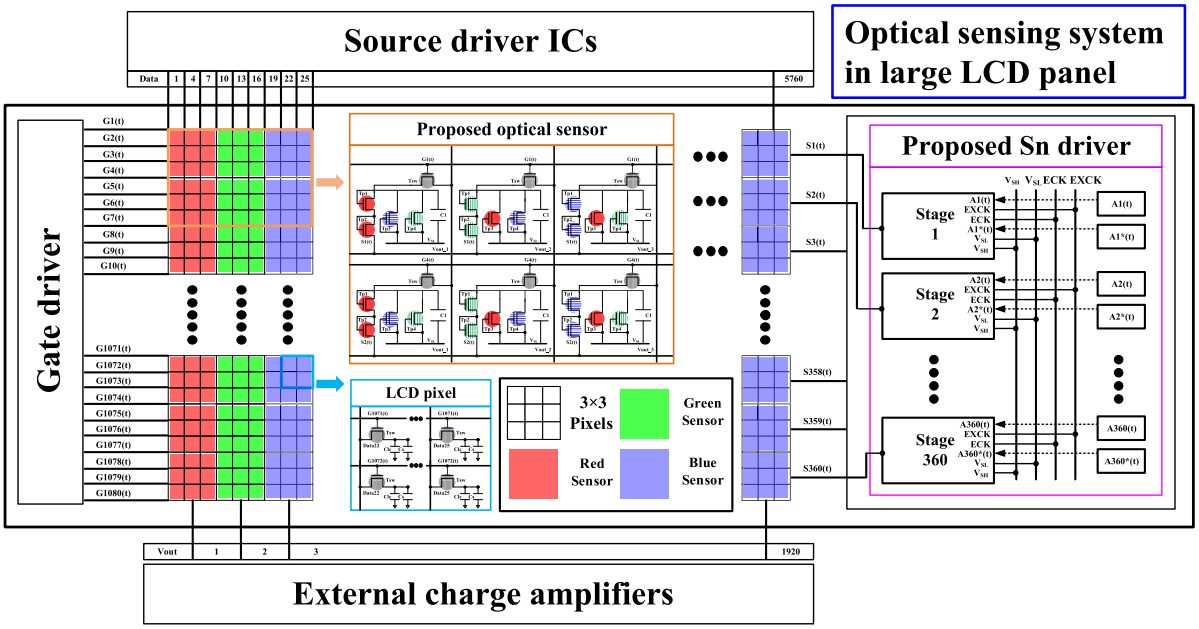

FIGURE 2. Array architecture of proposed optical sensors integrated with driver circuits in large LCD panel.

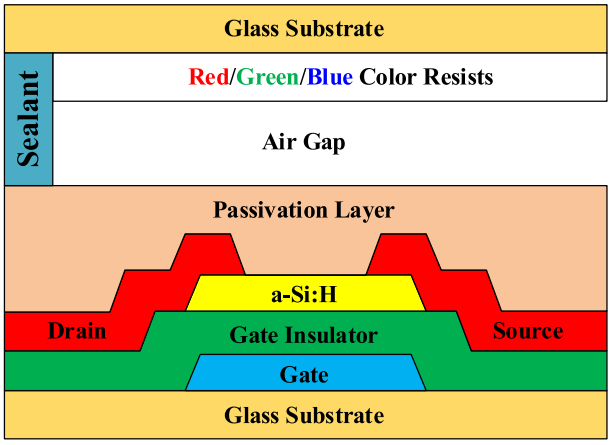

FIGURE 3. Cross-sectional view of standard a-Si:H TFT device with color filters.

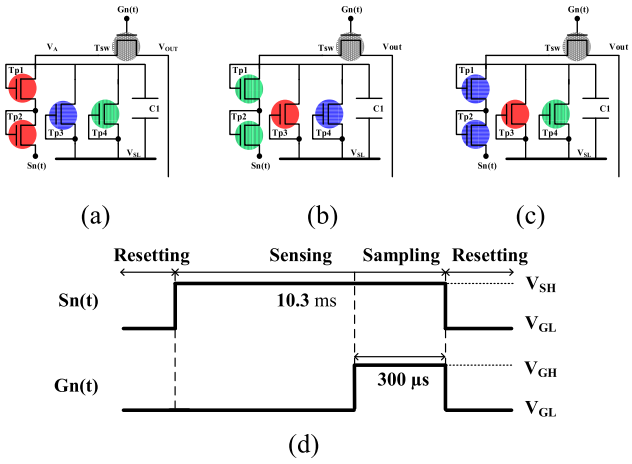

FIGURE 4. Proposed optical sensors for detecting light of three primary colors. (a) Red light. (b) Green light. (c) Blue light. (d) Corresponding timing diagram.

presents the corresponding timing diagrams of three types of proposed optical sensors. Two sensing photo TFTs with a series-connected structure yield half the V_{DS} stress of one sensing photo TFT in the original WPCG structure, improving the long-term degradation of the sensing photo TFT. Another two photo TFTs generate the compensating photocurrent to suppress the effect of variations in the ambient white light on the detection results of the optical sensor. Since the three types of optical sensors have similar structures and operations, the red optical sensor is an example introduced as follows.

Fig. 5(a) presents the operation of the proposed optical sensor in the resetting stage. Sn(t) changes to VSL to turn on Tp1 and Tp2, resetting the charges in the storage capacitor, so the V_A node is at the low voltage of $V_{SL} + V_{TH\_Tp1} + V_{TH\_Tp2}$, where V_{TH_Tp1} and V_{TH_Tp2} represent the threshold voltages of Tp1 and Tp2, respectively. During the sensing stage, Sn(t) switches from V_{SL} to V_{SH} to turn off Tp1 and Tp2. The amount of photocurrent that is generated by photo TFTs that are illuminated with red light or ambient white light determines the voltage of the V_A node. Fig. 5(b) shows the illumination of the optical sensor by red light. Tp1 and Tp2 generate a large photocurrent, resulting in a large V_{DS} of Tp3 and Tp4. Thus, the storage capacitor is charged to a high voltage. In contrast, the sensing photocurrent that is generated under ambient white light is lower than that under red light,

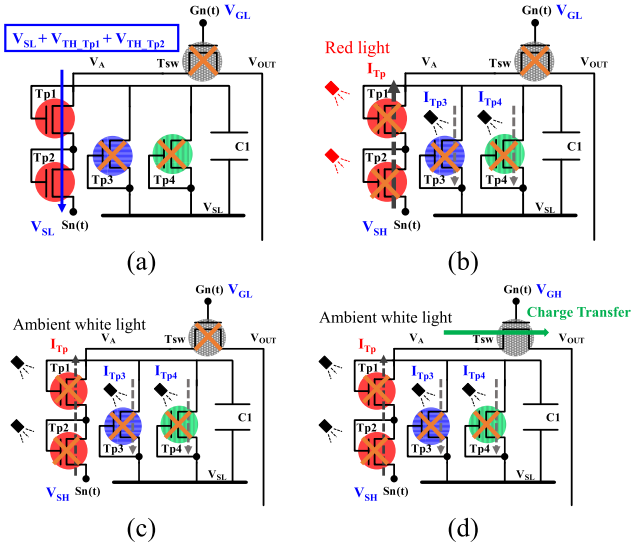

FIGURE 5. Operation of red optical sensor. (a) Resetting stage. (b) Sensing stage with red light. (c) Sensing stage under ambient white light. (d) Sampling stage.

as shown in Fig. 5(c). Therefore, a small induced photocurrent yields a low V_{DS} of Tp3 and Tp4, and the V_A node can be maintained at a low voltage. The series-connected structure of Tp1 and Tp2 yields half of the large V_{DS} stress that is achieved using only one sensing TFT in the original WPCG structure, which suffers from large V_{DS} stress. The reliability of the optical sensor is thus improved. In the sampling stage shown in Fig. 5(d), Gn(t) goes to V_{GH} to activate Tsw, so the stored charges in the storage capacitor are transmitted to an external charge amplifier. The differences between the output voltages of the optical sensor with and without an optical signal can be determined to realize binary detection of the optical signal with the multi-position sensing function.

B. PROPOSED DRIVER CIRCUIT AND ITS OPERATION

Fig. 6 presents the schematic and timing diagram of the newly proposed driver circuit that has two output generation structures (T1-T6, C1, and T7-T12, C2) and one pull-down structure (T13-T16, C3). An(t) and An*(t) are used to control the output period duration of the output waveforms with a large pulse width. ECK and EXCK are the low-frequency clock signals that switch between two of the modes of the driving TFTs (T3 and T9). Either the output waveforms are generated or the V_{TH} shifts are recovered by negative bias stress during the sensing stage. V_{SH} and V_{SL} are the high and the low voltage of the system, respectively.

In the first frame operation of the proposed driver circuit, ECK and EXCK are respectively at V_{GH} and V_{GL} to determine the modes of T3 and T9. During the initial output stage, An(t) switches to V_{GH} to turn on T1, T2, T7, T8, T15, and T16, so nodes Qn(t), Kn(t), and Pn(t) are respectively charged or discharged to $V_{GH}- V_{TH\_T1}$, V_{SL}, and V_{SL}. Thus, T3 is enabled to transmit V_{DD} fully to the row line.

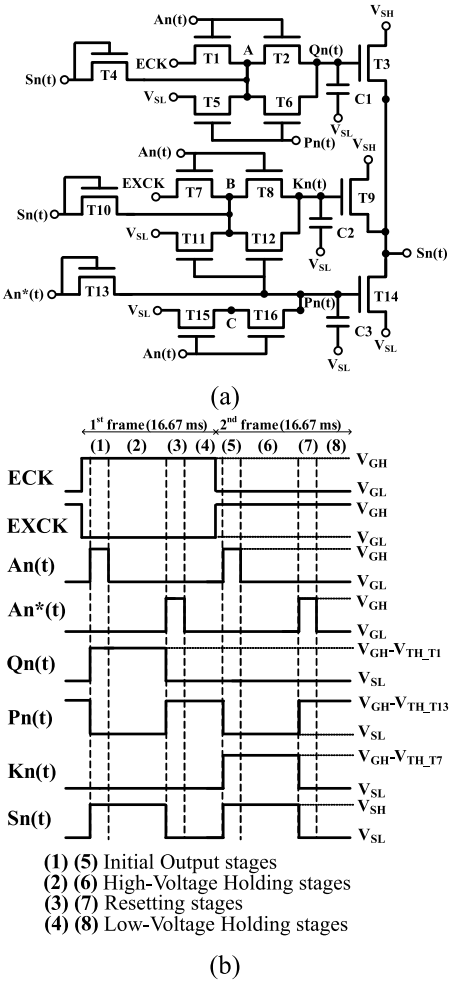

FIGURE 6. Proposed driver circuit. (a) Schematic diagram. (b) Timing diagram.

After the initial output stage, An(t) changes from V_{GH} to V_{GL} to turn off T1, T2, T7, T8, T15, and T16. Because the high-voltage holding stage lasts as long as 10.3 ms, the leakage currents of the switching TFTs easily affect the voltage of node Qn(t), reducing the driving capability of T3 and distorting the output waveform. To avoid the above-mentioned issues, the leakage current prevention structure that consists of two series-connected structures and one diode-connected structure is used in the switching TFT. Two series-connected structures of T1, T2, T5, and T6 protect the voltage of node Qn(t) from the leakage currents. The diode-connected structure of T4 continuously charges node A to $V_{DD}–V_{TH\_T4}$ by signal Sn(t) to decrease the V_{DS} of T2 and T6 for the lower leakage current until the end of the high-voltage holding stage. Thus, node Qn(t) is maintained at a high voltage to ensure the driving capability of T3. Furthermore, T9 is simultaneously operated at negative bias stress to recover the V_{TH} shifts. In the resetting stage, An*(t) changes from V_{GL} to V_{GH} to turn on T13, so node Pn(t) is charged to $V_{GH} – V_{TH\_T13}$. Sn(t) is discharged to V_{SL} through T14.

Simultaneously, nodes Qn(t) and Kn(t) are discharged to V_{SL} by T5, T6, T11, and T12 to turn off T3 and T9, ensuring a stable row line. During the low-voltage holding stage, only An*(t) switches to V_{GL} to turn off T13, and the operation of the driver circuit remains constant. Consequently, Sn(t) is an output waveform with a large pulse width that can be generated to drive an optical sensor.

In the second frame, ECK and EXCK are respectively at V_{GL} and V_{GH} to switch the modes of T3 and T9. During the initial output and high-voltage holding stage, nodes Kn(t), Qn(t), and Pn(t) are respectively charged or discharged to $V_{GH} - V_{TH\_T7}$, V_{SL}, and V_{SL} by signal An(t). T9 is turned on to fully transmit V_{DD} to the row line, and T3 is operated at negative bias stress to recover the V_{TH} shifts. The operation of the proposed circuit in the resetting and low-voltage holding stages of the second frame is the same as that of the first frame. Thus, node Pn(t) is still charged to $V_{GH} - V_{TH\_T13}$ by signal An*(t) to turn on T14, ensuring that the row line is discharged to V_{SL}, which is maintained until the next frame. Based on the above-mentioned operations, the optical sensor and driver circuit promote stability and increase the lifetime of the optical sensing system for use in large AMLCDs.

III. RESULTS AND DISCUSSION

A. RELIABILITY ANALYSIS OF PROPOSED WPCG STRUCTURES

To compare the WPCG structures of the optical sensors in the previous and the present works shown in Figs. 7(a), 7(b), 7(c), and 7(d), in terms of long-term stability, four a-Si:H photo TFTs are covered with a red filter and are measured under four stress conditions and the illumination of 4,000 lux at 70 °C. The aspect ratio of 60 μm/ 8 μm for the red photo TFTs is used only to ensure that the initial characteristics of the optical sensor are similar. Fig. 7(e) shows the degradation of photocurrents of the sensing photo TFTs under various stress conditions associated with the WPCG structures. First, the stress voltages V_{GS} and V_{DS} are set to 0 V and 25 V, respectively, to simulate the sensing photo TFT of the original WPCG structure during the sensing stage without an optical signal [12]. The photocurrents are measured every 24 h at a V_{GS} of 0 V and a V_{DS} of 25 V. The photocurrent degradation of the first sensing photo TFT after 120 h is 3.71 nA. Next, the second sensing photo TFT is used under 50% duty bias stress to imitate the sensing photo TFT [15], and the degradation of the photocurrent as a result of long-term stress is 1.59 nA. The third sensing photo TFT under stress by a negative V_{GS} of -0.5 V and a V_{DS} of 25 V is used to model the sensing photo TFT [16], and the photocurrent is measured repetitively. The degradation of the photocurrent is then found to be 1.25 nA. For the proposed WPCG structure with series-connected sensing TFTs, the stress and measurement conditions are V_{GS} of 0 V and V_{DS} of 12.5 V. The photocurrent degradation of the fourth sensing photo TFT after 120 h is 1.03 nA, which is smaller than 1.59 nA and 1.25 nA in the previously developed WPCG structures [15], [16]. To evaluate the reliability of

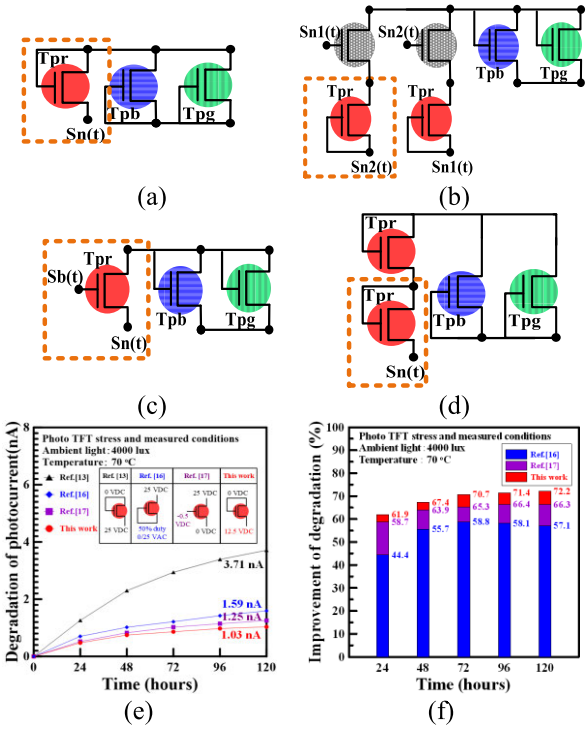

FIGURE 7. Primary sensing photo TFT in previously and newly proposed WPCG structures. (a) [12]. (b) [15]. (c) [16]. (d) This work. (e) Degradation of photocurrents of sensing photo TFTs under various stress conditions. (f) Improvement of degradation of photocurrents relative to original WPCG structure.

the WPCG structure, the reduction of the degradation of the sensing photo TFT is calculated as follows.

$$\text{Improvement}\,(\%) = \frac{I_{DO} - I_{DP}}{I_{DO}} \times 100\% \qquad (1)$$

where I_{DO} is the degradation of the photocurrent of the sensing photo TFT in the original WPCG structure, and I_{DP} is the degradation of the photocurrent of the sensing photo TFT in the previously developed or newly proposed WPCG structures. Fig. 7(f) presents the improvements for the previously developed and newly proposed WPCG structure. After 120 h, the improvement of the degradation of the sensing photo TFT that is based on the newly proposed structure is 72.2%, which exceeds the values of 66.3% and 57.1% that were previously achieved. Table 1 compares the conventional optical sensor with other optical sensors with original and improved WPCG structures. As a result, unlike the previously developed structures that require one set of additional sensing structures or an additional signal line, the degradation of the sensing photo TFT that uses only one additional photo TFT is successfully suppressed, and the improvement is higher than 5.9%, verifying the effectiveness and stability of the proposed WPCG structure to improve the lifetime of the optical sensing system.

B. MEASUREMENT SYSTEM

To investigate the reliability and integration of the optical sensing system, an optical sensor and a driver circuit are

TABLE 1. Comparison between conventional, previous and newly developed sensors.

Optical sensors	SID [14]	IEEE EDL [12]	IEEE TIE [15]	IEEE Access [16]	Proposed Method
Sensor structure	2T1C	5T1C	8T1C	4T1C	**5T1C**
Signal line	2	2	3	3	**2**
Type of sensing optical signal	1	3	3	3	**3**
Suppressing effect of ambient light	N/A	Yes	Yes	Yes	Yes
Improving reliability Method	N/A	N/A	50% duty V_{DS} stress	Negative V_{GS} stress	**Halving V_{DS} stress**
Improvement of degradation (Sensing photo TFT)	N/A	N/A	2.12 nA (57.1%)	2.46 nA (66.3%)	**2.68 nA (72.2%)**
Additional structure for WPCG	N/A	Original WPCG	3T & 1 signal line	0T & 1 signal line	**1T**
Sn driver circuit for optical sensor	One set	One set	Two sets	Two sets	**One set**

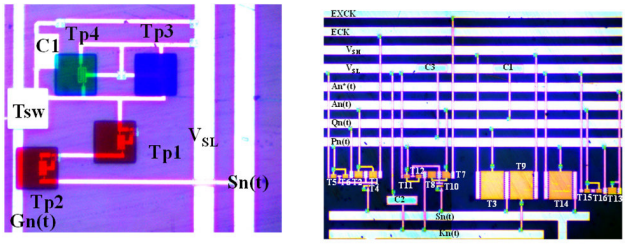

(a) (b)

FIGURE 8. Optical images of (a) proposed optical sensor, and (b) proposed driver circuit.

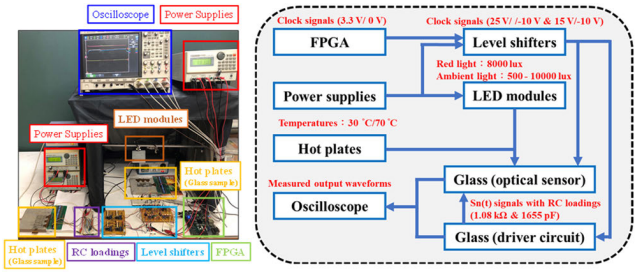

FIGURE 9. Platform of measurement system.

fabricated. Fig. 8 presents optical images of the fabricated sensor and driver circuit. Due to the floating of the V_A node of the optical sensor, an inverter-type readout circuit [12], [15], [16] is also used to avoid probe loading of the oscilloscope, which would directly affect the measured results. Table 2 and Table 3 present the design parameters of the fabricated sensors and driver circuits. The RC loadings are set to 1.08 kΩ and 1655 pF for a 65-inch display panel with a resolution of 1920 × 1080 and a frame rate of 60 Hz. Fig. 9 shows the system for measurements of the optical sensor and driver circuit, including a field programmable gate array (FPGA), level shifters, an oscilloscope, hot plates, LED modules, and power supplies. The FPGA is used to generate the required signals such as Gn(t), An(t), An*(t), ECK, and EXCK, and the level shifters which integrate power supplies, adjust the voltage of the signals from 3.3 V and 0 V to 25 V and -10 V. The output signals from level shifters and direct-current voltages from the connected power supplies are applied to our proposed circuits. The LED module provides the required optical signals and ambient white light with different illumination intensities. The hot plate controls the temperature throughout a long-term reliability test. The oscilloscope is used to measure the output waveforms of the proposed optical sensor and driver circuit.

TABLE 2. Parameters of proposed optical sensor.

Design parameters	Values
Tp1, Tp2, Tp3, Tp4	60 μm/8 μm
Tsw	60 μm/6 μm
C1	3 pF
V_{GH}	25 V
V_{GL}, V_{SL}	-10 V
Sn(t)	-10 to 15 V
Gn(t)	-10 to 25 V

TABLE 3. Parameters of proposed driver circuit.

Design parameters	Values
T1, T2, T7, T8, T13	400 μm/5.5 μm
T3, T9, T14	6000 μm/5.5 μm
T4, T10	10 μm/5.5 μm
T5, T6, T11, T12, T15, T16	100 μm/5.5 μm
C1, C2, C3	4 pF
V_{SH}	15 V
V_{SL}	-10 V
An(t), An*(t), ECK, EXCK	-10 to 25 V

C. FUNCTIONALITY AND RELIABILITY OF OPTICAL SENSING SYSTEM

Fig. 10 plots the output voltages of the proposed optical sensor with an inverter-type readout circuit under various light intensities during the sampling period. The red light is set to 8000 lux. The resolution of the optical sensing system is set to 1 bit for realizing the highly robust binary detection. The output voltages of Sn(t) are at 14.79 V and 14.77 V in two consecutive frames. The output voltages of the proposed optical sensor are respectively 13.93 V and -4.9 V,

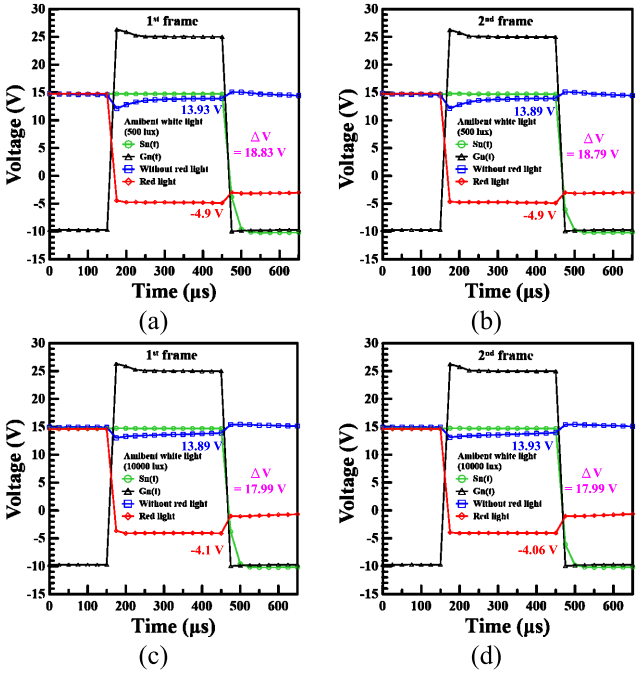

FIGURE 10. Measured output voltages of proposed optical sensor and driver circuit with and without red light under ambient white light of various intensities. (a) First frame and (b) Second frame under illumination by ambient white light of 500 lux. (c) First frame and (d) Second frame under illuminations by ambient white light of 10,000 lux.

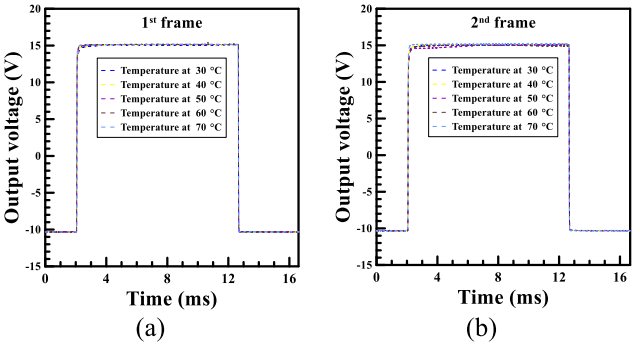

FIGURE 11. Measured waveforms of Sn(t) at different temperatures. (a) First frame. (b) Second frame.

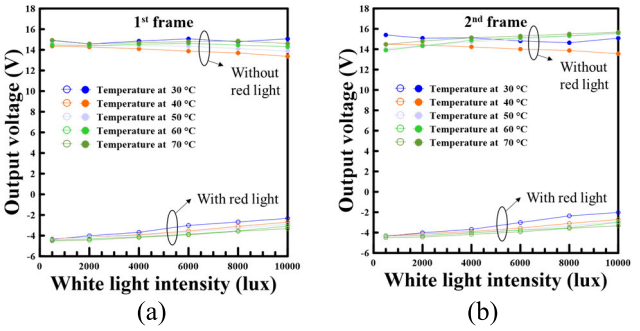

FIGURE 12. Measured output voltages of proposed optical sensor with and without red light at different temperatures. (a) First frame. (b) Second frame.

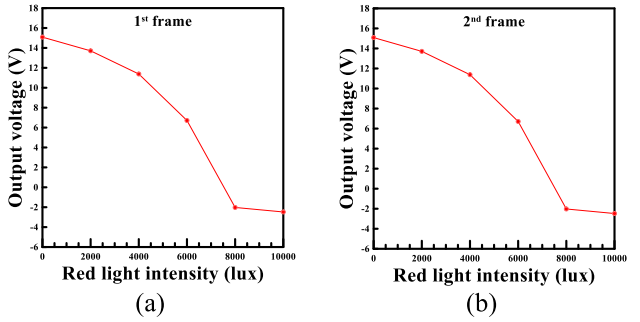

FIGURE 13. Measured output voltages of proposed optical sensor with red light of various intensities under illumination intensity of ambient white light of 10000 lux. (a) First frame. (b) Second frame.

and 13.89 V and -4.9 V, with and without red light in two consecutive frames under ambient white light with a low intensity of 500 lux. When the intensity of the ambient white light is increased to a high value of 10000 lux, the differences in the output voltage with and without red light are maintained at 17.99 V in the two consecutive frames, proving the high immunity of the proposed optical sensor to ambient white light.

Fig. 11 and 12 present the output waveforms and voltages of the proposed optical sensor and driver circuit in the two consecutive frames at different temperatures. The output waveforms of the driver circuit are almost similar as the measured temperatures increase from 30 °C to 70 °C. The minimum difference in the output voltage of the optical sensor is 16.06 V, ensuring the functionality of the optical sensing system. Thus, the proposed sensors and driver circuits operate normally under temperature variations.

Fig. 13 shows the output voltages of the proposed optical sensor with various illumination intensities of red light under the intensity of the ambient white light of 10000 lux. To evaluate the sensing characteristics of the optical sensing system, the sensitivity is calculated as follows.

$$\text{Sensitivity} = \frac{\Delta V_{out}}{\Delta Lx_{red}} \left(\frac{mV}{lux}\right) \tag{2}$$

where ΔV_{out} is the variation of the output voltage, and ΔLx_{red} is the variation of the intensities of the red light. Table 4 indicates the sensitivity of the optical sensing system. The sensitivity of the optical sensing system in two consecutive frames is almost similar, proving the reliable sensing function of the proposed sensing system at high illuminations of ambient white light. Furthermore, Fig. 14 presents the output voltage of the proposed optical sensor with the various illumination intensities of red light and ambient white light. To realize highly robust binary detection, the intensity of red light of 8000 lux is suitable as the optical signal for the sensing range of ambient white light from 500 lux to 10000 lux.

Fig. 15 and 16 demonstrate the long-term reliability of the proposed optical sensor and driver circuit in the two

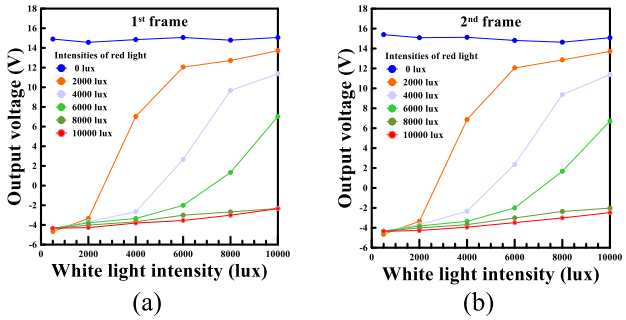

FIGURE 14. Measured output voltages of proposed optical sensor with various illumination intensities of red light under varying ambient white light intensities. (a) First frame. (b) Second frame.

TABLE 4. Sensitivity of optical sensing system in two consecutive frames.

Ambient white light = 10000 lux					
Red light / Frame	0-2000 (lux)	2000-4000 (lux)	4000-6000 (lux)	6000-8000 (lux)	8000-10000 (lux)
1st	-0.68 mV/lux	-1.17 mV/lux	-2.17 mV/lux	-4.68 mV/lux	-0.01 mV/lux
2nd	-0.69 mV/lux	-1.16 mV/lux	-2.33 mV/lux	-4.37 mV/lux	-0.23 mV/lux

TABLE 5. Voltage drops of Sn(t) signal and minimum differences in output voltages of optical sensors in two consecutive frames.

Measured output voltages of waveforms of proposed driver circuit									
Stress time (hours)	Initial	72	144	216	288	360	432	504	576
1st frame (V)	14.79	14.75	14.75	14.75	14.75	14.75	14.73	14.73	14.73
Voltage drops(%) (Ideal：15 V)	1.4%	1.67%	1.67%	1.67%	1.67%	1.67%	1.8%	1.8%	1.8%
2nd frame (V)	14.77	14.75	14.75	14.75	14.75	14.75	14.75	14.73	14.72
Voltage drops(%) (Ideal：15 V)	1.53%	1.67%	1.67%	1.67%	1.67%	1.67%	1.67%	1.8%	1.87%
Minimum differences in output voltages of proposed optical sensor									
Stress time (hours)	Initial	72	144	216	288	360	432	504	576
1st frame (V)	18.58	19.39	19.35	19.33	19.71	19.44	19.58	19.32	19.54
2nd frame (V)	18.60	19.33	19.35	19.33	19.71	19.46	19.58	19.32	19.53

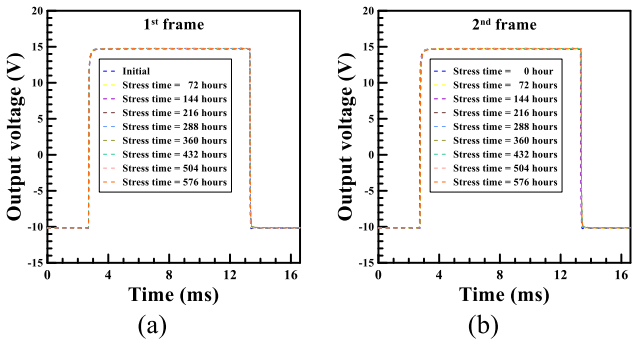

FIGURE 15. Measured waveforms of Sn(t) during a 576 h long-term and high-temperature reliability test. (a) First frame. (b) Second frame.

consecutive frames. To accelerate the lifetime test, the temperature and the ambient white light of the test environment are set at 70 °C and 4000 lux, respectively. After the continuous application for long-term stress of 576 h, the proposed driver circuit still generates stable output waveforms that drive the optical sensor. Table 5 also shows that the output

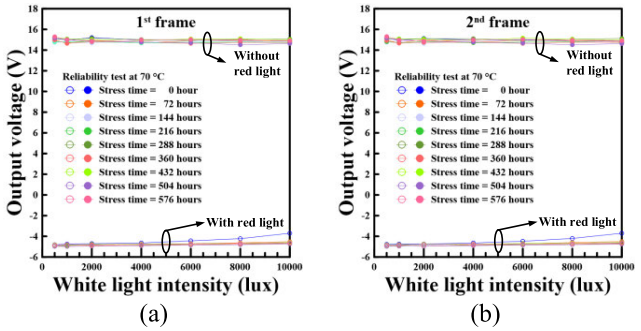

FIGURE 16. Measured output voltages of proposed optical sensor with and without red light during a 576 h long-term and high-temperature reliability test. (a) First frame. (b) Second frame.

voltages of the waveforms are kept at 14.73 V and 14.72 V in two consecutive frames after long-term stress, demonstrating that the voltage drops are less than 1.87%. Moreover, the minimum difference in the output voltage of the proposed optical sensor between two consecutive frames is 18.58 V under ambient white light from 500 lux to 10000 lux, revealing the reliability and successful integration of the proposed optical sensor and driver circuit. Accordingly, the newly proposed WPCG structure enhances the reliability of the optical sensor and can be successfully integrated with a driver circuit to realize an optical sensing system with a long lifetime.

IV. CONCLUSION

This study develops a lifetime optimization of optical sensing system that is integrated with highly reliable optical sensors and driver circuits that are based on a-Si:H TFTs. It realizes a multi-position sensing function without a complex algorithm or an additional sensing module by integrating into conventional a-Si:H TFTs and color filter technologies without any additional photolithographic mask or processing step in the fabrication. To extend the lifetime of the optical sensing system, the optical sensor with a series-connected structure of two sensing photo TFTs halves the V_{DS} stress, reducing the degradation of the two photo TFTs. Unlike in previous works, only one set of Sn driver circuits is required in the proposed WPCG structure, so the number of required ICs can be reduced, reducing the cost of the AMLCD. In addition, the driver circuit using the alternately controlled and leakage current prevention structures increases the stability of the required output waveforms of the optical sensor. The experimental results demonstrate that the degradation of the photocurrent that is associated with the fabricated photo TFT is suppressed from 3.71 nA to 1.03 nA, and the improvement of the degradation of the photocurrent after 120 h is 72.2%, which exceeds the values of 66.3% and 57.1% that have been achieved in the previous works. The minimum difference in the output voltage of the optical sensor is 16.06 V as the measured temperatures vary from 30 °C to 70 °C. The proposed driver circuit generates stable output waveforms, whose voltage drops are less than 1.87% between two con-

secutive frames. The minimum difference between the output voltages of the optical sensor after long-term operation for 576 h at 70 °C with and without an optical signal is 18.58 V. Based on these results, the optical sensor with the driver circuit increases the lifetime of the optical sensing system and performs highly robust optical sensing functions in large AMLCDs.

ACKNOWLEDGMENT

AUO Corporation is appreciated for its technical support.

REFERENCES

[1] B.-D. Choi and O.-K. Kwon, "Line time extension driving method for a-Si TFT-LCDs and its application to high definition televisions," *IEEE Trans. Consum. Electron.*, vol. 50, no. 1, pp. 33–38, Feb. 2004, doi: 10.1109/TCE.2004.1277838.

[2] J. Yang, C. Liao, K. Wang, J. An, S. Shen, and S. Zhang, "A-Si TFT integrated gate driver workable at −40 ∘C using bootstrapped carry signal," *IEEE Access*, vol. 10, pp. 93887–93893, 2022, doi: 10.1109/ACCESS.2022.3204149.

[3] C.-L. Lin, F.-H. Chen, M.-X. Wang, P.-C. Lai, and C.-H. Tseng, "Gate driver based on a-Si:H thin-film transistors with two-step-bootstrapping structure for high-resolution and high-frame-rate displays," *IEEE Trans. Electron Devices*, vol. 64, no. 8, pp. 3494–3497, Aug. 2017, doi: 10.1109/TED.2017.2710180.

[4] Z. Hu, C. Liao, W. Li, L. Zeng, C.-Y. Lee, and S. Zhang, "Integrated a-Si:H gate driver with low-level holding TFTs biased under bipolar pulses," *IEEE Trans. Electron Devices*, vol. 62, no. 12, pp. 4044–4050, Dec. 2015, doi: 10.1109/TED.2015.2487836.

[5] L.-W. Chu, P.-T. Liu, and M.-D. Ker, "Design of integrated gate driver with threshold voltage drop cancellation in amorphous silicon technology for TFT-LCD application," *J. Display Technol.*, vol. 7, no. 12, pp. 657–664, Dec. 2011, doi: 10.1109/JDT.2011.2162937.

[6] B. Hekmatshoar, "Electrical stability and flicker noise of thin-film heterojunction FETs on poly-Si substrates," *IEEE Access*, vol. 7, pp. 77063–77069, 2019, doi: 10.1109/ACCESS.2019.2921233.

[7] H.-J. Chiu and S.-J. Cheng, "LED backlight driving system for large-scale LCD panels," *IEEE Trans. Ind. Electron.*, vol. 54, no. 5, pp. 2751–2760, Oct. 2007, doi: 10.1109/TIE.2007.899938.

[8] K. Wang, H. Ou, and J. Chen, "Dual-gate photosensitive thin-film transistor-based active pixel sensor for indirect-conversion X-ray imaging," *IEEE Trans. Electron Devices*, vol. 62, no. 9, pp. 2894–2899, Sep. 2015, doi: 10.1109/TED.2015.2457449.

[9] M. Xu, H. Li, H. Ou, J. Chen, S. Deng, N. Xu, and K. Wang, "Dual-gate photosensitive a-Si:H TFT array enabling fingerprint-sensor-integrated display application," *J. Display Technol.*, vol. 12, no. 8, pp. 835–839, Aug. 2016, doi: 10.1109/JDT.2016.2540814.

[10] Y.-H. Tai, L.-S. Chou, Y.-F. Kuo, and S.-W. Yen, "Gap-type a-Si TFTs for backlight sensing application," *J. Display Technol.*, vol. 7, no. 8, pp. 420–425, Aug. 2011, doi: 10.1109/JDT.2011.2135838.

[11] C. J. Brown, H. Kato, K. Maeda, and B. Hadwen, "A continuous-grain silicon-system LCD with optical input function," *IEEE J. Solid-State Circuits*, vol. 42, no. 12, pp. 2904–2912, Dec. 2007, doi: 10.1109/JSSC.2007.908695.

[12] C.-L. Lin, C.-E. Wu, P.-S. Chen, C.-H. Chang, C.-C. Hsu, J.-S. Yu, C. Chang, and Y.-H. Tseng, "Hydrogenated amorphous silicon thin-film transistor-based optical pixel sensor with high sensitivity under ambient illumination," *IEEE Electron Device Lett.*, vol. 37, no. 11, pp. 1446–1449, Nov. 2016, doi: 10.1109/LED.2016.2607235.

[13] C. W. Kuo, Y. Y. Liao, L. H. Tsai, S.-P. Lu, M.-F. Chiang, Y.-C. Lin, and J.-S. Yu, "44-1: Photo sensors embedded within TFT-LCD with three primary colors optical touch function," in *SID Symp. Dig. Tech. Papers*, Jun. 2019, vol. 50, no. 1, pp. 600–603, doi: 10.1002/sdtp.12992.

[14] A. Abileah, W. den Boer, T. Larsson, T. Baker, S. Robinson, R. Siegel, N. Fickenscher, B. Leback, T. Griffin, and P. Green, "59.3: Integrated optical touch panel in a 14.1' AMLCD," in *SID Symp. Dig. Tech. Papers*, May 2004, vol. 35, no. 1, pp. 1544–1547, doi: 10.1889/1.1821371.

[15] C.-L. Lin, C.-E. Wu, C.-L. Lee, F.-H. Chen, Y.-S. Lin, W.-L. Wu, and J.-S. Yu, "Alternately controlled optical pixel sensor system using amorphous silicon thin-film transistors," *IEEE Trans. Ind. Electron.*, vol. 66, no. 9, pp. 7366–7375, Sep. 2019, doi: 10.1109/TIE.2018.2880718.

[16] F.-H. Chen, C.-L. Lee, J.-H. Chang, W.-S. Liao, C.-A. Lin, C.-W. Kuo, and C.-L. Lin, "Long-term behavior of hydrogenated amorphous silicon thin-film transistors covered with color filters for use in optical sensors," *IEEE Access*, vol. 7, pp. 116172–116178, 2019, doi: 10.1109/ACCESS.2019.2936405.

[17] J. W. Choi, J. I. Kim, S. H. Kim, and J. Jang, "Highly reliable amorphous silicon gate driver using stable center-offset thin-film transistors," *IEEE Trans. Electron Devices*, vol. 57, no. 9, pp. 2330–2334, Sep. 2010, doi: 10.1109/TED.2010.2054453.

[18] C. Liao, Z. Hu, D. Dai, S. Chung, T. S. Jen, and S. Zhang, "A compact bi-direction scannable a-Si:H TFT gate driver," *J. Display Technol.*, vol. 11, no. 1, pp. 3–5, Jan. 2015, doi: 10.1109/JDT.2014.2366782.

[19] C.-L. Lin, M.-H. Cheng, C.-D. Tu, C.-C. Hung, and J.-Y. Li, "2-D–3-D switchable gate driver circuit for TFT-LCD applications," *IEEE Trans. Electron Devices*, vol. 61, no. 6, pp. 2098–2105, Jun. 2014, doi: 10.1109/TED.2014.2319096.

[20] C.-L. Lin, M.-H. Cheng, C.-D. Tu, C.-E. Wu, and F.-H. Chen, "Low-power a-Si:H gate driver circuit with threshold-voltage-shift recovery and synchronously controlled pull-down scheme," *IEEE Trans. Electron Devices*, vol. 62, no. 1, pp. 136–142, Jan. 2015, doi: 10.1109/TED.2014.2372820.

CHIH-LUNG LIN (Senior Member, IEEE) received the M.S. and Ph.D. degrees in electrical engineering from National Taiwan University, Taiwan, in 1993 and 1999, respectively. He is currently a Professor with the Department of Electrical and Engineering, National Cheng Kung University, Tainan, Taiwan. His current research interests include pixel circuit design for AMOLED and BPLCD, gate driver circuit design for AMLCD, and flexible display circuits.

CHIA-LUN LEE received the B.S. and M.S. degrees in electrical engineering from National Cheng Kung University, Tainan, Taiwan, in 2016 and 2018, respectively, where he is currently pursuing the Ph.D. degree in electrical engineering. His current research interests include gate driver circuit design for AMLCD, pixel circuit design for AMOLED, and optical pixel sensor circuit design.

CHENG-HAN KE received the B.S. degree in electrical engineering from National Cheng Kung University, Tainan, Taiwan, in 2021, where he is currently pursuing the Ph.D. degree in electrical engineering. His research interests include the system circuit design for mini-LED and micro-LED displays.

PO-CHENG LAI received the B.S. degree in electrical engineering from Feng Chia University, Taichung, Taiwan, in 2014, and the M.S. and Ph.D. degrees in electrical engineering from National Cheng Kung University, Tainan, Taiwan, in 2016 and 2022, respectively. He is currently with AU Optronics Corporation, Hsinchu, Taiwan, working on the AMOLED panel design. His research interests include pixel circuit, gate driver circuit, and system design for AMOLED displays and AMLCDs.

CHUNG-TIEN CHIU received the B.S. degree in electrical engineering from National Cheng Kung University, Tainan, Taiwan, in 2022, where he is currently pursuing the M.S. degree in electrical engineering. His research interests include the system circuit design for mini-LED and micro-LED displays.

YU-CHANG CHIU received the B.S. degree in electrical engineering from National Cheng Kung University, Tainan, Taiwan, in 2023, where he is currently pursuing the M.S. degree in electrical engineering. His research interests include the system circuit design for mini-LED and micro-LED displays.

CHIA-WEI KUO received the B.S. and Ph.D. degrees from the Department of Physics, National Cheng Kung University, Tainan, Taiwan, in 2001 and 2006, respectively. In 2006, he joined the Industrial Technology Research Institute (ITRI), Hsinchu, Taiwan, for the development of flexible LCD project. In 2011, he joined the Advanced Display Optical Research Department, AU Optronics Corporation (AUO), as the Manager. He has been mainly working on pixel circuit design and architectures for advanced displays.